XX IMEKO World Congress
Metrology for Green Growth
September 9–14, 2012, Busan, Republic of Korea

FEM SIMULATION ON AERODYNAMIC CHARACTERISTICS OF INRIM FORCE LABORATORY

D. Quagliotti, A. Germak, A. Piccato, and P. G. Spazzini

Istituto Nazionale di Ricerca Metrologica (INRIM), Torino, Italy, D.Quagliotti@inrim.it

Abstract: In this paper a methodology for estimating the airflow effects in deadweight force standard machines, using simulations with finite elements method, is proposed.

Simulating the environment of the INRIM force laboratory, influenced by the air-conditioning system, has allowed to determine probable aerodynamic characteristics of the ambience housing the masses systems under study. Furthermore, the simulations revealed the probable airflow effects on a INRIM forthcoming deadweight force standard machine.

Keywords: FEM simulation, airflow, force, deadweight force standard machine.

1. INTRODUCTION

After introductory studies [1-2] on the possibility of simulating with the finite elements method (FEM) the system of masses of a deadweight force standard machine (dFSM), we adopted a systematic approach to FEM simulation on the aerodynamic characteristics of the underground room of INRIM force laboratory (where the masses systems are situated) with the aim of providing a methodology for the evaluation of airflow effects in dFSMs.

Aerodynamic effects investigated in this paper are due to the forces exerted by the dynamic interaction of the generated air motion onto the surface of the masses. In fact, the air-conditioning surge coming from the inflows exits the room through four openings towards the ground floor, generating a consistent airflow (figure 1).

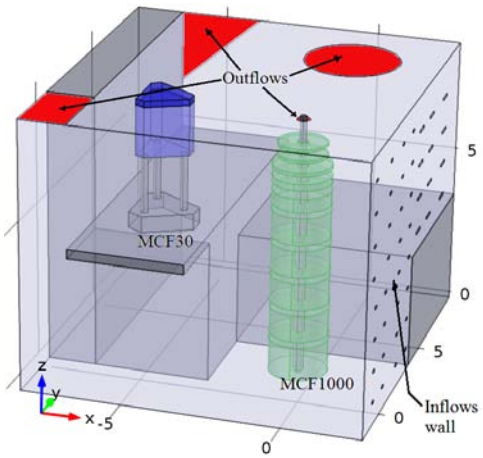

Fig. 1. Picture of the basement of the INRIM force laboratory. MCF1000 masses, MCF30, outflows and inflows are visible.

Airflow is an influence factor which is usually considered negligible, nevertheless we propose a general method for its verification. In fact, airflow could be somewhat deceitful under certain conditions and the knowing of how it acts may be particularly helpful to detect critical issues, as well as in the design and installation of new dFSMs.

For this purpose, we have estimated the effects due to the air-conditioning flow on the INRIM dFSM Galdabini 1 MN (MCF1000) and on a new dFSM of capacity 100 kN (nMCF100), designed at INRIM, whose construction is planned in the upcoming years. Another dFSM, the Galdabini 30 kN (MCF30), was also considered in the simulation environment but not in the evaluation because it is completely shielded from the airflow: closed in the side surface and also in the upper hole (figures 1 and 2).

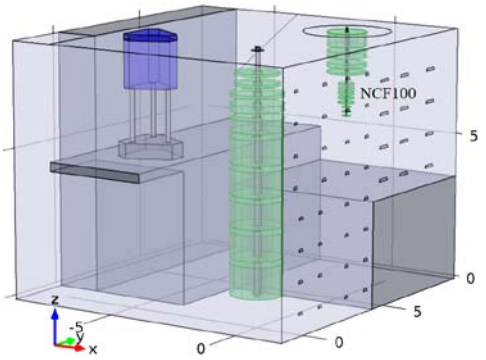

Fig. 2. The basement provided with the nMCF100.

2. THE ENVIRONMENT SIMULATED

The MCF1000 extends in depth from the ground floor to the basement. As shown in figures 1 and 2, the basement is organized in three different levels.

One level is occupied by the MCF1000 masses. In another level the masses of MCF30 are stacked. Finally, the remaining level will be for the nMCF100 (it is dealt in separate simulations).

The nozzles are all arranged on one wall of the basement. Thirty-two nozzles of size (180 × 80) mm blow towards MCF1000 masses. Other twelve nozzles are of size (480 × 80) mm and their level corresponds to that intended for the nMCF100 (figures 1 and 2). So the masses are

directly exposed to inflows, as qualitatively shown in figure 3.

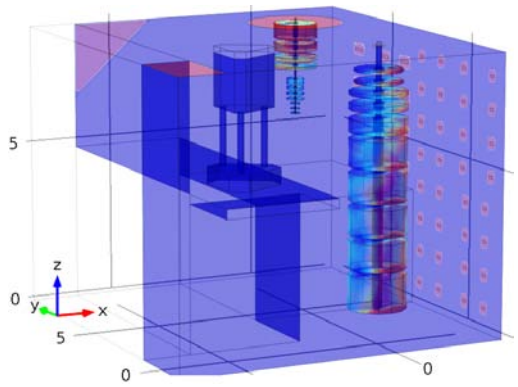

Fig. 3. Airflow on MCF1000 and nMCF100 masses (qualitative). The red colour highlights the prevalent airflow course.

The inflows direction is normal to the wall where the nozzles are, whereas the outflows direction is prevalent vertical.

Velocities in the region of the first MCF1000 mass were measured by experimental sessions of about four days with two hot-wire anemometers in different conditions [2]. In turn, representative maximum values were chosen with a vane anemometer (TESTO brand, model 445). The values used in the simulations are 1.6 m/s for the small nozzles and 0.6 m/s for the big ones.

The whole location housing the masses systems was considered. The modelling of the dFSMs under study was limited to the masses systems with the central rod of the loading frame.

3. AERODYNAMIC CHARACTERISTICS

The simulations were conducted in the worst case, first on the MCF1000. Then, the nMCF100 was laid down and the simulations were repeated to calculate approximately the consequence of the perturbed ambience in the presence of the new dFSM.

For the MCF1000 the worst case corresponds to the airflow that acts on the smaller mass which generates a nominal force of 10 kN. In the nMCF100, instead, the smaller mass would have an effective surface exposed to the flow that is too reduced for a significant result. So, for the nMCF100, the worst case should be when the airflow acts on the smaller mass of the bigger ones. That mass will generate a nominal force of 6.4 kN.

The temperature in the basement is controlled at each different level. As a result the temperature gradient can be considered negligible and, consequently, there is no free convection [3]. An ambient temperature of 293.15 K was considered.

The reference pressure used in the simulation was 988.5 Pa, that is the mean value of the ambient pressure measured at INRIM in the period from 2001 to 2006. The total pressure in the simulation ambience is considered as the sum of the reference pressure with the pressure deviation due to the air-dynamics.

The velocities for the two types of nozzles are imposed by the air-conditioning system. Since these simulations are expected to emulate the macroscopic behaviour of the systems in the worst case, the velocities considered were the maximum ones with no time variations. For this reason, the estimated deviations from the dFSMs generated forces are to be intended as the maximum appreciable.

3.1. Simulation with Finite Element Method (FEM)

The tool used for the analysis is a commercial FEM software (COMSOL Multiphysics® ver. 4.2a). In particular, the airflow was modelled using the *Laminar Flow Module* (LFM) with incompressible Navier-Stokes equations and, given the small velocities involved, without any model of turbulence. Moreover, the numerical *consistent* stabilization techniques *streamline diffusion* (Galerkin Least-Squares) and *crosswind diffusion* were used, introducing artificial diffusion in the flow direction and orthogonally, respectively. Streamline diffusion allows to use first order elements for both pressure and velocity in the discretized model; crosswind diffusion improves the resolving of sharp boundary layers and shear layers. This consistent techniques do not perturb the original transport equation.

Being this one a stationary non linear complex system, the convergence is difficult to achieve because of the inseparability of parasitic time dependent solutions excited due to numerical noise [4], as a result the solutions could be someway dependent upon initial conditions. For this reason, preliminary rough solutions for first estimates of some initial guesses were used to advantage the convergence. Furthermore, the available LFM option *Pseudo Time Stepping* was used, which is a fictitious time derivative to improve the solution to the transient problem of the stationary formulation.

At the boundaries the tangential component of velocity was imposed continuous across the solid-fluid interfaces. This is called *no-slip condition*.

For a viscous fluid, in certain conditions across a solid-fluid interface, a zero velocity for the fluid results at the boundary. In fact, the particles in the flow would tend to adhere to the walls of the solid interface. So, if the solid is not moving, the tangential component of the fluid velocity at the surface must be zero. If the solid-fluid interface does not deform, the normal component must also be zero.

Although the no-slip condition is normally used in modelling of viscous flows, in this case, with the masses immersed in the incoming fluid, it appears that the velocity of the fluid at the borders with the masses could also be non-zero. For this reason, the simulations were repeated both with the no-slip condition and with the *slip condition* (only for the masses systems), i.e. allowing that the velocity may also be non-zero at the boundaries with the masses.

Such an extended system in 3D modelling contains items that are rather differentiated in the dimension scale, so the mesh becomes inevitably composite and dense especially when discretizing the boundary layers. The maximum element size for defining the boundary layers was imposed

of 0.1 m down to a minimum of 10^{-6} m. Overall, the finer mesh (see below) was of about 3×10^6 elements, allowing in the volume the same minimum size of the boundary layers. Therefore, great computational effort is required to carry out the simulations. In order to deal with this overhead a nonlinear solver (Newton's method; rel. toll. 10^{-5}) was coupled with an iterative FGMRES and a geometric *multigrid* methods which use a hierarchy of two levels mesh. In this way, the system is preliminary solved on a coarse mesh with a parallel direct solver algorithm (PARDISO) combined with pre- and post-conditioners (SSOR - relaxation factor $\omega = 0.9$). Every few iterations this solution is prolonged on a finer mesh by the iterative solver (V cycle). It is then assembled and the nonlinear solver works out the overall solution.

Finally, the aerodynamic vertical force (lift) was computed as difference of the integral of the pressure on the bottom face of the mass under observation minus the integral of the pressure on the top one. Such value represents the overall spurious force deriving from aerodynamic effects, i.e. the sought error in the nominal force.

3.2. Results considering only the MCF1000

Figure 4 shows the deviation of the pressure field (volume) distributed in the basement, due to the airflow, with respect to the reference pressure, and the velocity field (black arrows). The average pressure deviation is about 7.4 mPa. The mean value of the magnitude of the velocity field in the volume is about 0.034 m/s. In the picture, to increase the visibility, the arrows length is ten times the value of the velocity components.

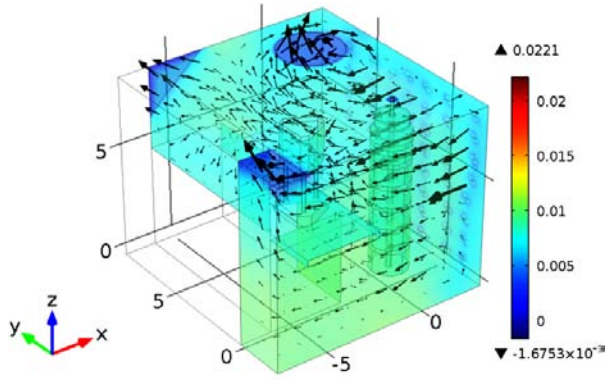

Fig. 4. Coloured volume stands for the pressure (Pa) and the black arrows are ten times proportional to the velocity field.

The lift deriving from the pressure deviation acts as a disturbance on the 10 kN mass and introduces a relative error on its generated force. Considering the "no-slip" case, this error is relatively small (table 1).

In the "slip" case, an increment of the lift is observed which led to a relative error in the generated force of about 0.1 ppm. This error can still be considered negligible (table 1).

Table 1. Relative error in the generated force Er_10 considering the 10 kN mass on the MCF1000, in the two cases treated.

Boundary conditions on masses	$E_{r\ 10}$ ($\times 10^{-6}$)
No-slip	0.053
Slip	0.097

The prevailing direction of the airflow path, qualitatively shown in the figure 3, is confirmed in figures 5 and 7 which report the distribution of the lift on the mass under study. The consequence is an overturning moment on the mass.

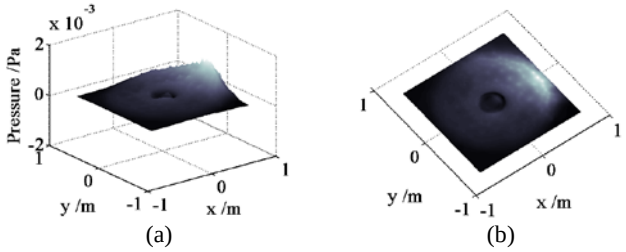

(a) (b)

Fig. 5. No-slip: pressure deviation on the MCF1000 10 kN mass. (a) axonometric view. (b) top view.

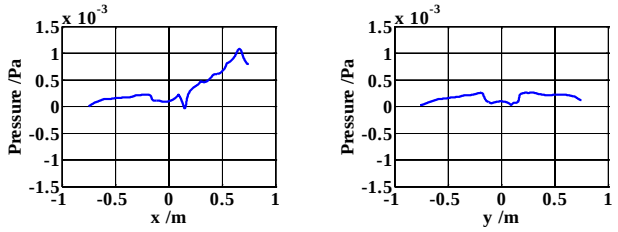

(a) (b)

Fig. 6. No-slip: pressure deviation on the MCF1000 10 kN mass. (a) diameter of the mass in the plane y=0. (b) diameter of the mass in the plane x=0.

Figures 6 represent the figures 5 sliced, respectively, with a y=0 plane and with a x=0 plane.

The following figures 7 and 8 relate the slip case.

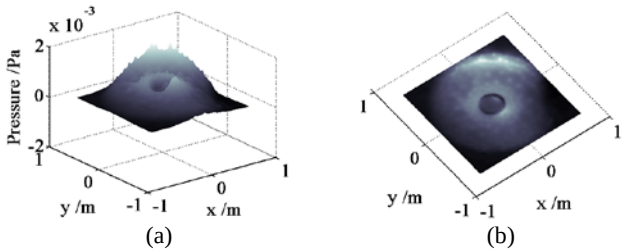

(a) (b)

Fig. 7. Slip: pressure deviation on the MCF1000 10 kN mass. (a) axonometric view. (b) top view.

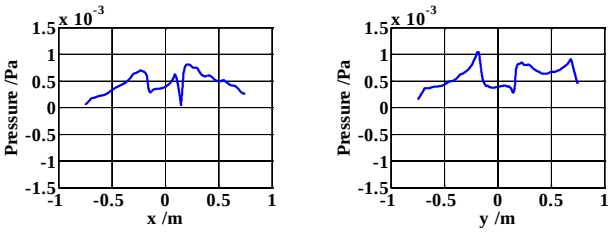

(a) (b)

Fig. 8. Slip: pressure deviation on the MCF1000 10 kN mass.
(a) diameter of the mass in the plane y=0.
(b) diameter of the mass in the plane x=0.

3.3. Results adding the nMCF100

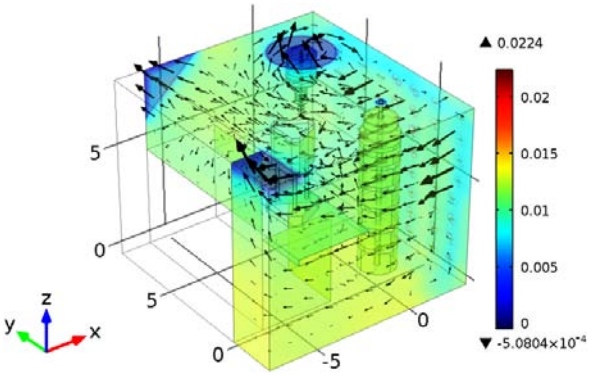

Fig. 9. Coloured volume stands for the pressure (Pa) and the black arrows are ten times proportional to the velocity field.

When the nMCF100 is added to the simulation environment, the large round outflow is significantly reduced (figures 2 and 9). The consequence is a slight decrease of the average velocity (0.028 m/s) and an increase of the average pressure deviation up to about 8.5 mPa. Nevertheless the increment is mostly evident on the 6.4 kN mass of the nMCF100. It seems that the reduced outflow focuses this increment and that the MCF1000 takes advantage from this dislocation (table 2).

Table 2. Relative error in the generated force Er_6.4, considering the 6.4 kN mass on the nMCF100, and Er_10, considering the 10 kN mass on the MCF1000, in the two cases treated.

Boundary conditions on masses	$E_{r\ 6.4}$ ($\times 10^{-6}$)	$E_{r\ 10}$ ($\times 10^{-6}$)
No-slip	0.15	0.013
Slip	0.27	0.026

Comparing the two no-slip cases, without and with the nMCF100, we note, in fact, that, when the nMCF100 is considered in the simulation environment, the lift effect on the 10 kN mass of the MCF1000 is translated downwards.

In the simulated environment conditions, it worth to note that the 6.4 kN mass, as well as all the nMCF100 masses, would be completely invested by the airflow, getting out from the corresponding outlet, which might be likely to develop a certain level of vorticity separated from the downstream wake. This vorticity would have the effect of an additional disturbance on the upper masses.

The following figures 10-17 show the two no-slip and slip cases, respectively, on the MCF1000 10 kN mass and, then, on the nMCF100 6.4 kN mass.

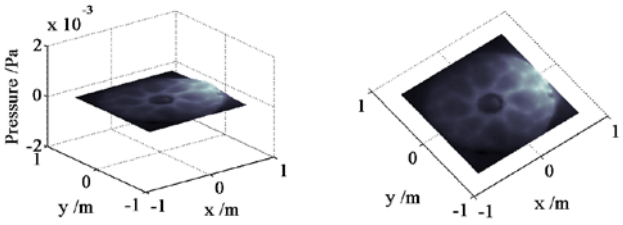

(a) (b)

Fig. 10. No-slip: pressure deviation on the MCF1000 10 kN mass.
(a) axonometric view. (b) top view.

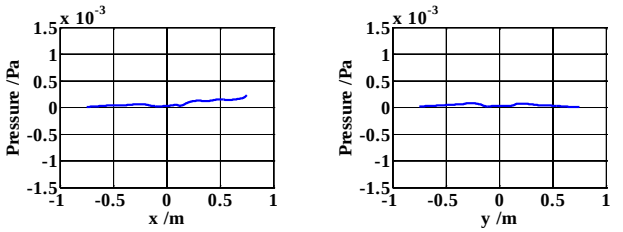

(a) (b)

Fig. 11. No-slip: pressure deviation on the MCF1000 10 kN mass.
(a) diameter of the mass in the plane y=0.
(b) diameter of the mass in the plane x=0.

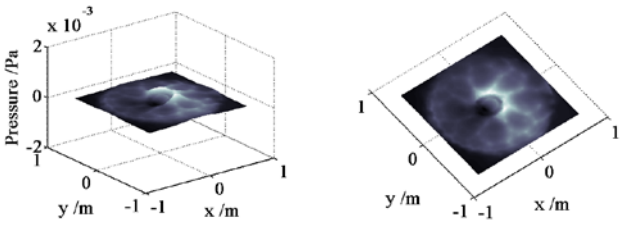

(a) (b)

Fig. 12. Slip: pressure deviation on the MCF1000 10 kN mass.
(a) axonometric view. (b) top view.

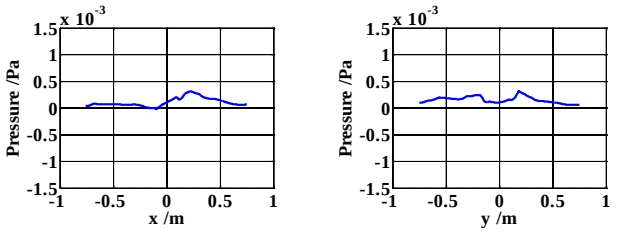

(a) (b)

Fig. 13. Slip: pressure deviation on the MCF1000 10 kN mass.
(a) diameter of the mass in the plane y=0.
(b) diameter of the mass in the plane x=0.

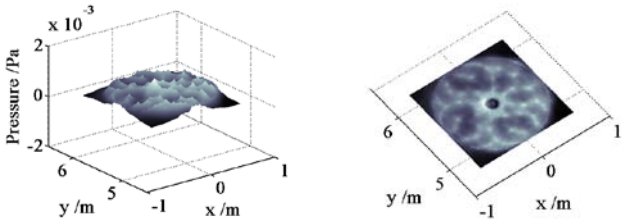

(a) (b)

Fig. 14. No-slip: pressure deviation on the nMCF100 6.4 kN mass. (a) axonometric view. (b) top view.

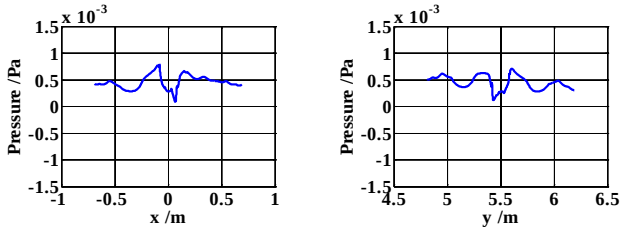

(a) (b)

Fig. 15. No-slip: pressure deviation on the nMCF100 6.4 kN mass. (a) diameter of the mass in the plane y=0. (b) diameter of the mass in the plane x=0.

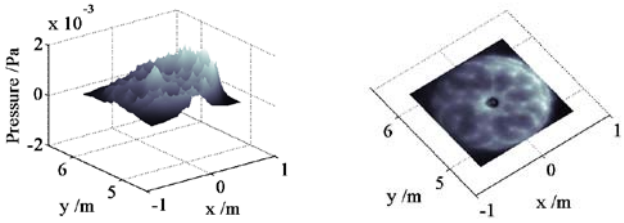

(a) (b)

Fig. 16. Slip: pressure deviation on the nMCF100 6.4 kN mass. (a) axonometric view. (b) top view.

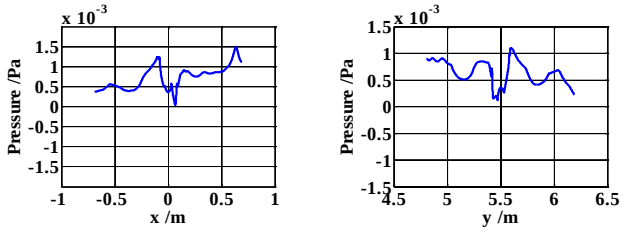

(a) (b)

Fig. 17. Slip: pressure deviation on the nMCF100 6.4 kN mass. (a) diameter of the mass in the plane y=0. (b) diameter of the mass in the plane x=0.

3.4 Solving considerations

When a system is particularly sensitive to initial conditions, that system is called *complex*. The transverse instability in airflow at high Reynolds numbers leads to a complexity of the motion.

In the system under study, on the masses where the evaluations were made, the Reynolds number is definitely low (40-60) but its maximum in the entire volume reaches (MCF1000) and exceeds (when nMCF100 is added) by far 3000. Furthermore, the FEM model is complicated by a dependency of the nonlinear stationary solver on initial guesses. Hence some complexity to complete the solution is certainly present and it was also observed during first simulations.

Even though this affects other parts of the system that are not those under investigation, particular attention has to be paid to get a solution that represents a stable state of the system. A system is stable if a small perturbation (e.g. numerical noise) does not move to another state far from the initial one. The danger is that the ambiguity of the initial conditions leads to a system that is not distinguishable from a stochastic one.

A *chaotic attractor*, in fact, is also a state (unstable) of the dynamic system which, deterministically, is known in the phase space as the trajectory of the solution starting from some initial state. However, it is not uniquely defined since the attractor is an *asymptotic state*: a lot of initial conditions can be attracted even after a long time towards this state. States that are greatly distant initially may become nearby eventually.

A state represents the all degrees of freedom of the system so that it is repeatable in its definition of a model. For a FEM model this implies to give a time dependency to a model that is stationary or periodic [4].

Consequently, if on one hand the assumption of a stationary model helps to avoid the ken of the dynamics of the air source, on the other it adds complexity to the system.

In order to avoid unsettled computational models, the final solutions were achieved by stepwise, repeating the simulations with different meshes, different solvers and different initial conditions (see figure 18 for an example of convergence). At last, the velocity of the simulated models demonstrated an encouraging numerical agreement with the experimental measurements in [2] which might represent a support in the modelling and solving of such simulations.

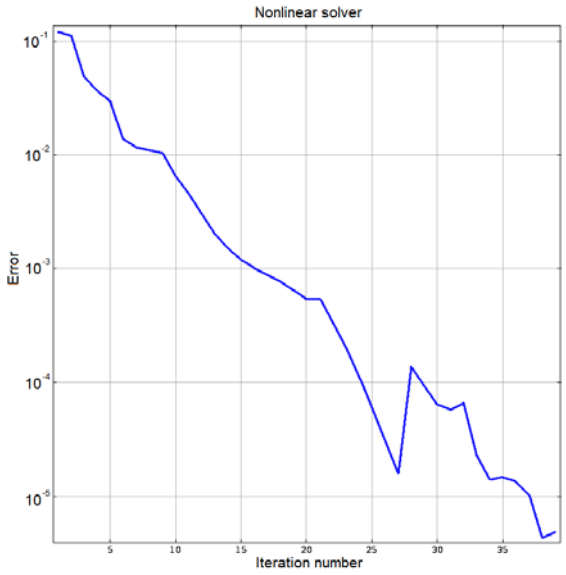

Fig. 18. Relative tolerance of the non linear stationary solver as a function of the solution steps.

4. CONCLUSIONS

The behaviour of the airflow is not easily determinable. It appears clear that closing the openings, if it would be natural to do, could have the unintended effect of increasing the pressure deviation and, as a consequence, the spurious force on the masses. The best solution is to shield the masses as in MCF30 and, when possible, to set up outflows that are far enough from the masses systems.

Moreover, though the probable behavior is better described by the no-slip condition, the slip condition can be considered as an upper limit, even if unreachable, to the expected value of the disturbance on the generated force.

The approach proposed in this paper is an estimate of what could happen to a dFSM in a ventilated environment and does not intend to predict the real airflow behaviour. It could help in the determining of critical issues both in designing and in installation of dFSMs and, if anything, it represents an approximate evaluation of the magnitude order of the disturbances due to airflow.

Again, a dense mesh is helpful for the success of such simulations but the computational effort required has a limit strictly connected with the machine hosting the calculation. It limits above all the mesh resolution with which the boundary layers can be modelled.

The multigrid method is an efficient algorithm to stretch these restrictions. Even so, a processing limit is always present, particularly when there aren't symmetries in the geometry that can reduce the 3D modelling to 2D.

For this reason, secondary (from the simulation point of view) frames of dFSMs and other structures internal to the laboratory have been neglected in the model. Nevertheless, a good agreement among simulations and experimental measurements suggests that the model is adequate for the afore mentioned purposes.

5. REFERENCES

[1] D. Quagliotti, G. D'Agostino, A. Germak, F. Mazzoleni and G. Barbato, "Influence of the mutual gravitation attraction in a set of masses of deadweight machines" in Proc. of XIX IMEKO World Congress on fundamental and applied metrology, pp. 198-200, Lisbon, 2009, ISBN: 978-963-88410-0-1.

[2] D. Quagliotti, A. Germak and F. Mazzoleni, "Influence of aerodynamic effects in deadweight machines", Poster of IMEKO 2010 TC3, TC5 and TC22 Conferences, Pattaya, 2010.

[3] C. Boffa, P. Gregorio, Elementi di Fisica Tecnica, Vol. II, Levrotto & Bella, Torino, 1976.

[4] W. B. J. Zimmerman, Process Modelling and Simulation with Finite Element Methods, World Scientific, Singapore, 2004.

[5] K. Koenig and Anatol Roshko, "An experimental study of geometrical effects on the drag and flow field of two bluff bodies separated by a gap", Journal of fluid mechanics, vol. 156, pp. 167-204, 1985.

[6] C. Norberg, "Flow around rectangular cylinders - pressure forces and wake frequencies", Journal of wind engineering and industrial aerodynamics, vol. 49, pp. 187-196, 1993, ISSN: 0167-6105.

[7] A. Sohankar, C. Norberg and L. Davidson, "Simulation of three-dimensional flow around a square cylinder at moderate Reynolds numbers", Physics of fluids, vol. 11, n. 2, pp. 288-306, 1999, ISSN: 1070-6631.

[8] A. Cakrawala and A. Umemura, "Experimental study on aerodynamic characteristics of a stepped-nose obstacle", Transactions of the Japan society for aeronautical and space sciences, vol. 46, pp. 238-245, 2004, ISSN: 0549-3811.